



Preparation and characterization of zirconium (1,3,5,2λ⁵,4λ⁵,6λ⁵-triazatriphosphinine-2,2,4,4,6,6-hexyl) hexa(phosphate) as a novel high-temperature proton conductor

Chuangang Wang¹ · Weihui Cui¹ · Peng Sun¹ · Zhongfang Li¹ · Yan Wang¹ · Hongchang Pei¹ · Xiaoyan Yin¹

Received: 7 September 2020 / Revised: 15 October 2020 / Accepted: 21 November 2020 / Published online: 7 January 2021
© Springer-Verlag GmbH Germany, part of Springer Nature 2021

Abstract

Zirconium (1,3,5,2λ⁵,4λ⁵,6λ⁵-triazatriphosphinine-2,2,4,4,6,6-hexyl) hexa(phosphate) (ZrTHPA) is synthesized by chelation combination (1,3,5,2λ⁵,4λ⁵,6λ⁵-triazatriphosphinine-2,2,4,4,6,6-hexyl) hexa(phosphonic acid) (THPA) with zirconium ion in a certain ratio. The THPA is synthesized by hexachlorocyclotriphosphazene with P(OEt)₃, and hydrolyzed in HCl. Their structure is characterized by nuclear magnetic resonance (NMR) and infrared spectroscopy (IR), and hydrogen bonding and chelation interactions between Zr⁴⁺ and phosphonic acid are detected. X-ray diffraction and scanning electron microscopy (SEM) show that ZrTHPA has a layered structure. Thermogravimetry-differential thermal analysis (TG-DTA) shows that ZrTHPA has good thermal stability. ZrTHPA also has good oxidative stability and hydrolysis resistance. The ion exchange capacity of ZrTHPA (1:2) is 2.21 meq g⁻¹. At 180 °C, the proton conductivity of ZrTHPA (1:2) at 100%, 50%, and 0 relative humidity is 0.128 S cm⁻¹, 0.069 S cm⁻¹, and 0.038 S cm⁻¹, respectively. ZrTHPA can be used as solid acid catalyst or proton conductor which is doped into proton exchange membranes.

Keywords Inorganic-organic composite proton acid · High-temperature proton conductor · ZrTHPA · Proton conductivity · Oxidative stability · Hydrolysis resistance

Introduction

Proton-conductive phosphates and phosphonates have received extensive research interest due to their applications in various chemical devices such as fuel cells and sensors [1–3]. When applied as proton conductors in fuel cells, their proton conductivity is among the key issues which determines the power conversion efficiency [4–6]. These proton conductors can be doped into polymer electrolytes of which the working temperature can be as high as 200 °C owing to their water-independent Grotthuss mechanism for proton transport [7–9].

Phosphoric acid (PA) has been commonly used as the proton conductor in polymer electrolytes, especially in polybenzimidazole-based ones [10–13]. However, PA

dehydrates into pyrophosphoric acid at high temperature and leaks from polymer electrolytes at high relative humidity (RH) [14, 15]. Additionally, increasing PA doping level causes deterioration of mechanical strength and dimensional stability while reducing PA doping level results in low proton conductivity [16, 17].

Inorganic metal phosphates and pyrophosphates were developed in the past few decades to address the issues mentioned above [18–22]. They are more stable at high temperature and do not leak at high RH. At moderate doping levels, they can improve the mechanical stability and dimensional property of the polymer electrolyte membranes [23, 24]. Nevertheless, their intrinsic inorganic structure induces phase separation with polymer matrixes at high doping levels, thus limiting their proton-conducting performances [24–26].

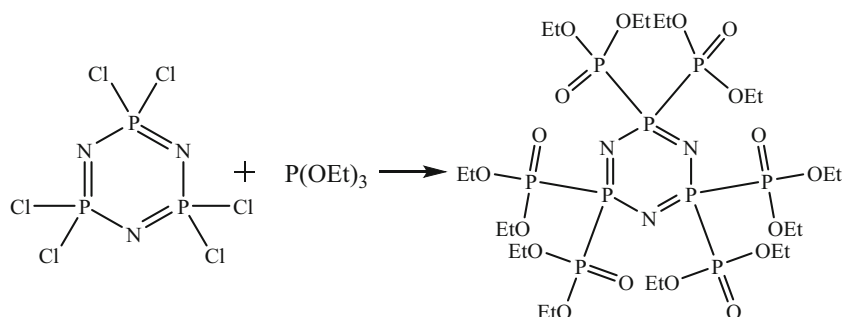
Organic-inorganic hybrids containing phosphoric acid or phosphonate moiety were chosen as the alternatives to improve the compatibility with polymer matrixes [27–29]. Their hybrid structure allows high doping levels and thus high proton conductivity.

Hexachlorocyclotriphosphazene (HCCP) has low melting point (112–115 °C) and good solubility in most organic

✉ Zhongfang Li
zhfli@sdu.edu.cn; lizhongfangzb@126.com

¹ School of Chemistry and Chemical Engineering, Shandong University of Technology, #266 Xincun West Road, Zibo City 255049, Shandong Province, People's Republic of China

Scheme 1 Synthetic route of DTHP. The ^1H NMR spectrum of DTHP (400 MHz, CDCl_3) δ = 1.247 (t, J = 7.2 Hz, 36H, CH_3), 3.727 (q, J = 7.2 Hz, 24H, CH_2)



solvents [18, 30, 31]. It has an aromatic ring although it has no carbon atoms, which exhibited good compatibility with polymers [22, 32–34]. The six P–Cl bonds in HCCP are highly active and are ready to undergo nucleophilic substitution reactions [30, 32, 35].

Inspired by the properties of phosphoric acid or phosphate-based proton conductors as well as by the good compatibility and reactivity of HCCP, six phosphoric acid groups were introduced into the HCCP backbone by a two-step reaction to synthesize (1,3,5,2 λ^5 ,4 λ^5 ,6 λ^5 -triazatriphosphinine-2,2,4,4,6,6-hexyl) hexa(phosphonic acid) (THPA). THPA was found to be water-soluble and thus its zirconium salt derivative ZrTHPA was prepared by chelation reaction between THPA and water-soluble zirconium salts (zirconyl chloride octahydrate).

The optimum performance of the proton conductor was obtained by screening the metal to acid ratios. The structure, morphology, and properties of ZrTHPA were studied, and the ion exchange capacity (IEC) and proton conductivity of proton conductors at high temperature and different RHs were measured.

Experimental

Materials

Hexachlorocyclotriphosphazene (HCCP, 99.0%) was purchased from Zeshi New Material Tech. Co., Ltd., triethyl phosphite (98%) was purchased from Tianjin Komio Chemical Reagent Co., Ltd., and zirconyl chloride octahydrate ($\text{ZrOCl}_2 \cdot 8\text{H}_2\text{O}$, 99 wt%) was purchased from

Sinopharm Group Chemical Reagent Co., Ltd. All raw materials meet the requirements without further purification.

Synthesis of DTHP

To a three-neck flask equipped with a condenser and a drying tube, triethyl phosphite (467.42 mmol, 55.83 mL) and HCCP (71.91 mmol, 25 g, in portions) under magnetic stirring were added. The reaction was exothermic and the solution gradually turned yellow. After complete addition, the temperature was raised to 120 °C and reacted for 6 h. After cooling, the product was extracted with petroleum ether to remove excess triethyl phosphite for 2–3 times, and dried at 90 °C in an oven to obtain a yellow viscous liquid which was DTHP (24.32 g, 25.41 mmol); the yield was 97.3%. The reaction equation is shown in Scheme 1. The structure of the compound was tested by nuclear magnetic resonance (NMR).

Synthesis of THPA

To a three-neck flask equipped with a condenser, a drying tube and a stirring rotor was added DTHP (24 g) and concentrated hydrochloric acid (150 mL) for stirring, then the mixture was heated to 120–140 °C for 72 h. Then, it was cooled, poured into a beaker, and concentrated to 40–50 mL at 120 °C. It was extracted for 2–3 times with appropriate amount of ethyl acetate to remove unhydrolyzed complete of DTHP, and dried at 140–160 °C in an oven to obtain a white transparent viscous liquid was THPA (22.58 g); the yield was 94.1%. The reaction equation is shown in Scheme 2. The

Scheme 2 Synthetic route of THPA. The ^{31}P NMR spectrum of DTHP (360 MHz CDCl_3) δ = –11.36 (3P, P=N), 0.43 (6P, $\text{PO}(\text{OH})_2$)

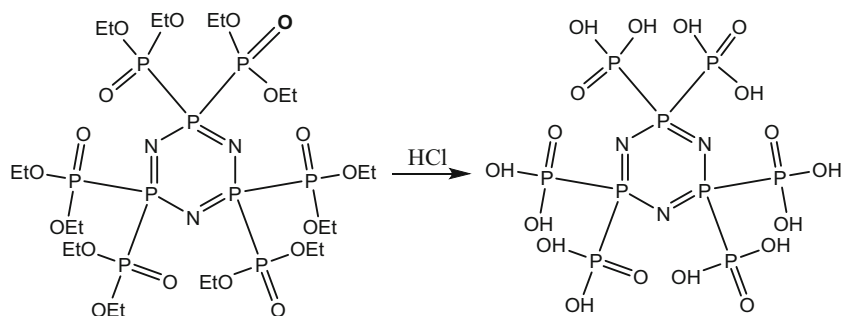


Table 1 Comparison of color, yield, IEC, and water uptake of THPA proton conductors

The molar ratio of Zr ⁴⁺ and THPA	The color of ZrTHPA	The yield of ZrTHPA	IEC (meq g ⁻¹)	Water uptake
1:1	White	87%	1.35	24%
3:4	White	74%	1.62	43%
2:3	White	62%	1.86	58%
1:2	White	54%	2.21	73%

structure of the compound was tested by nuclear magnetic resonance (NMR).

Synthesis of ZrTHPA

The obtained transparent viscous liquid (products in 2.3 above) (13.69 mmol, 8.5 g) was dissolved in water, and the corresponding zirconium oxychloride (6.84 mmol, 2.21 g) was dissolved in dilute hydrochloric acid, and each was dissolved completely. Under stirring, the zirconium oxychloride solution was added dropwise to the THPA solution. After the dropwise addition, the mixture was stirred for 24 h, filtered, washed to neutrality, and dried at 100 °C in an oven to obtain ZrTHPA(1:2). ZrTHPA (1:1, 3:4, 2:3, and 1:2) were prepared with the same method at different molar ratio of Zr⁴⁺ to THPA (Table 1). The structural formula of ZrTHPA is shown in Scheme 3.

Characterization

The structures of DTHP and THPA were determined by an NMR spectrometer (Bruke AVANCE III 400 MHz). The structure and intermolecular interactions of ZrTHPA were determined on a Nicolet 5700 FT-IR spectrometer (Thermo Electron Corporation) in transmission mode at room temperature by mixing the fine-powdered sample with KBr and pelleting. Transmittance (%) was recorded in the range of

4000–400 cm⁻¹ and 64 co-added scans were collected for each sample. The micromorphology of ZrTHPA was investigated applying SEM (FEI Sirion 200) and EDS. The elementary composition of ZrTHPA was confirmed from EDX (FEI Sirion 200). The thermal stability of ZrTHPA was measured using Netsch STA 409 thermogravimetric analyzer at a heating rate of 10 °C min⁻¹ from room temperature to 800 °C under an air flow of 30 mL min⁻¹. The XRD patterns with Cu K α radiation (40 mA, 40 kV) over a 2 θ range of 2°–60° were recorded on a Bruker D8 Advance diffractometer. By XRD peak position, the layer spacing is calculated by the following Eq. (1):

$$d = \frac{\lambda}{2\sin\left(\frac{2\theta}{2}\right)} \quad (1)$$

where λ (nm) is X-ray wavelength, Cu K α is 154.18 pm, 2 θ (°) is peak position, and d (nm) is layer spacing.

Water uptake, oxidative stability, hydrolysis resistance, and ion exchange capacity

The water uptake was measured by immersing 1.00 g of ZrTHPA in 20 mL deionized water at 80 °C for 24 h. Then, it was filtered, dried with tissue paper, and weighed.

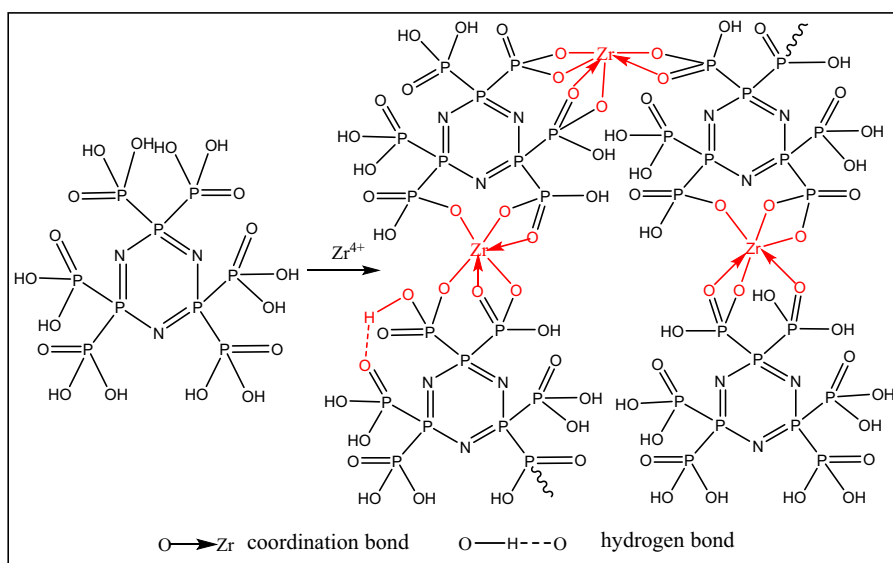
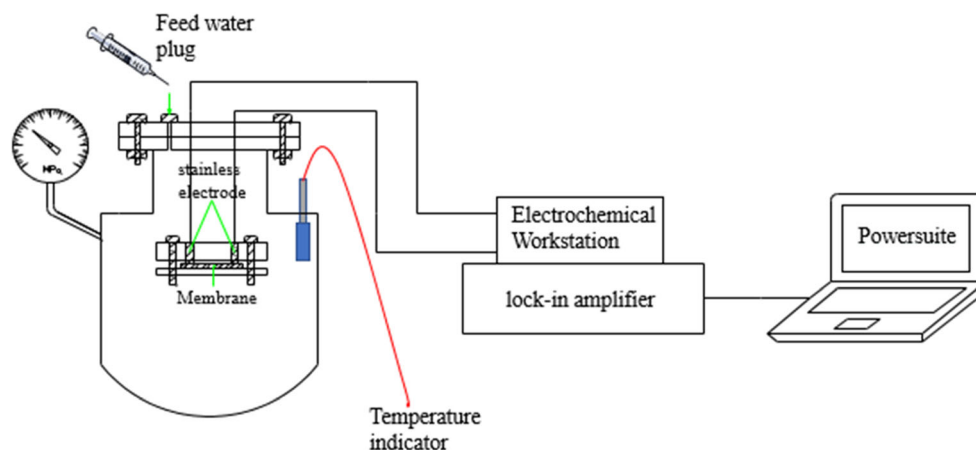
Scheme 3 Chemical structure of ZrTHPA (1:2)

Fig. 1 Measurement system of proton conductivity



The oxidative stability of ZrTHPA was measured by immersing 1.00 g of ZrTHPA in 20 mL Fenton reagent (3% H_2O_2 aqueous solution containing 5 ppm $(\text{NH}_4)_2\text{Fe}(\text{SO}_4)_2$) at 68 °C for 24 h. Then, it was filtered, dried, and weighed. Blank experiment was conducted by immersing powder in deionized water at 68 °C for 24 h. The deviation caused by dissolution was obtained by deducting weight loss of the blank experiment from the result of Fenton test.

The hydrolysis resistance in acidic conditions was measured by immersing 1.00 g of ZrTHPA in 0.1 M HCl aqueous solution at 80 °C for 24 h. Blank experiment was performed by immersing powder in deionized water at 80 °C for 24 h and the deviation caused by dissolution in water was deducted.

The IEC was measured by immersing 1.00 g of ZrTHPA in 50 mL saturated NaCl aqueous solution at 25 °C and magnetically stirred for 48 h. It was then filtered and the mother liquid was titrated using 0.01 mol L^{-1} NaOH aqueous solution. IEC (meq g^{-1}) was calculated from the following Eq. (2):

$$\text{IEC} = \frac{M \times V}{m} \quad (2)$$

where M (mol L^{-1}) is the concentration of NaOH aqueous solution, V (mL) is the volume of consumed NaOH aqueous solution, and m (g) is the mass of the sample.

Proton conductivity

To test the proton conductivity, powder was pressed into a sheet, clamped with the stainless electrodes and PTFE plates, and placed in a high-pressure autoclave [36]. The device is shown in Fig. 1. At 100% RH, the autoclave was prefilled with enough water and the pressure inside it was the saturated vapor pressure of water. At 50% RH, the actual pressure inside the autoclave was controlled by adjusting the amount of injection water from the injection port to let it reach half of the saturated vapor pressure of

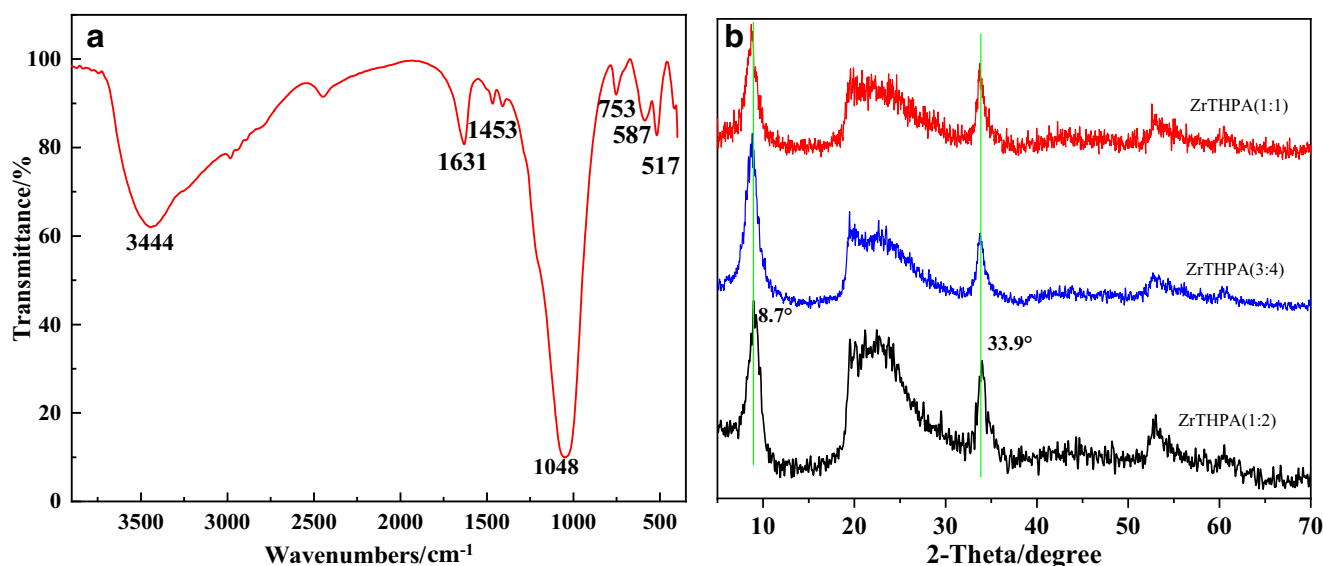
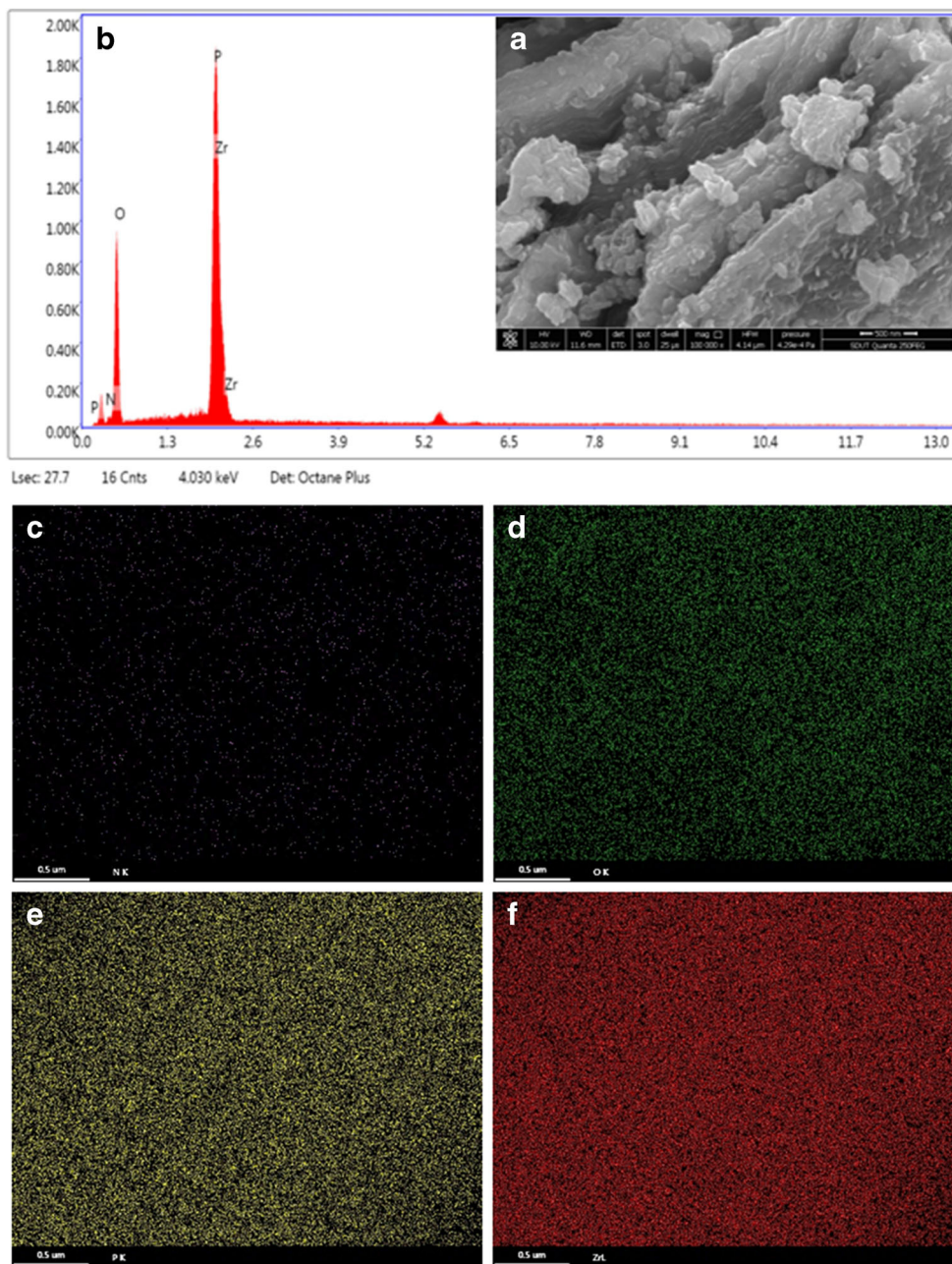


Fig. 2 FT-IR spectra (a) and XRD (b) spectra of ZrTHPA

Fig. 3 SEM (a), EDX (b), and the elementary of N (c), O (d), P (e), and Zr (f) images of ZrTHPA (1:2)



water. At 0 RH, it was measured in a drying oven. The resistance of the sample was obtained from AC impedance spectroscopy. Conductivities under different temperatures were calculated from the following Eq. (3):

$$\sigma = \frac{l}{AR} \tag{3}$$

σ (S cm⁻¹) is the membrane conductivity, l (cm) is the thickness of the sample, A (cm²) is the contact area between electrodes, and R (Ω) is the resistance.

Results and discussion

Fourier-transform infrared spectroscopy

The FT-IR spectrum of ZrTHPA (1:2) is shown in Fig. 2(a). The absorption peak at 3444 cm⁻¹ was caused by the hydroxyl groups in the phosphonic acid and the hydrogen bonds formed between them and P=O bonds. The absorption peak at 1631 cm⁻¹ was caused by the bending vibration of the bound water (H–O–H) between the layers. The absorption peak at 1453 cm⁻¹ was caused by the stretching vibration of P=O and

P=N bonds [37]. The broad absorption band at 1048 cm^{-1} was the tensile vibration absorption peak of P–P–O. The absorption peaks at 753 cm^{-1} , 587 cm^{-1} , and 517 cm^{-1} were caused by the synergistic effect of Zr^{4+} and THPA. The IR results demonstrated successful synthesis of the chelate of Zr and THPA.

X-ray diffraction

The XRD spectrum of ZrTHPA is shown in Fig. 2(b). It can be seen from the figure that the peak shapes of ZrTHPA are similar, and they are not an amorphous structure. And there was a sharp peak about 8.7° , indicated that the compound was a layered compound. Calculated by Eq. (1), the interlayer spacing of ZrTHPA (1:1, 3:4, 1:2) was 10.4, 10.28, and 10.16 nm, respectively. The average crystallite size of ZrTHPA(1:2) calculated by Scherrer was 42.2 nm. It can be seen from the figure that there was a sharp peak at 33.9° . It was known that this was the characteristic diffraction peak between Zr and O [38]. The peak positions of the other peaks were roughly the same with HCCP [39]. The XRD curve of ZrTHPA was different from any of the material structures reported in the literature, and it was known that a new compound was synthesized.

Scanning electron microscopy and energy-dispersive X-ray spectroscopy and mapping

The SEM and EDX micrographs are exhibited in Fig. 3(a) and 3(b). As can be seen from the SEM image (Fig. 3(a)), ZrTHPA has a granular shape. The compound contained P, O, N, and Zr elements, while Cl and C were not detected from EDX (Fig. 3(b)). P, O, N, and Zr were evenly distributed among them, without phase separation from the elementary mapping. The elemental composition of ZrTHPA was in good accordance with its chemical structure. In addition, ZrTHPA was not an amorphous structure from the XRD and SEM images.

Oxidative stability and hydrolysis resistance of ZrTHPA

The oxidative stability of ZrTHPA is shown in Fig. 4(a). After Fenton test, the remained weight of ZrTHPA (1:1, 3:4, 2:3, 1:2) was 96%, 93%, and 91%, 88%, respectively. It can be seen that as the relative content of THPA decreased, the oxidation stability of ZrTHPA increased, indicating that the main part affecting the stability of the substance was THPA rather than zirconium ion. The hydroxyl groups contained in THPA were susceptible to oxidative attack from hydroxyl radicals, which caused the generation of alkoxy groups and H_2O , thereby initiating the chain reactions [40]. Under the catalysis of zirconium ions, the free radicals induced the auto-oxidation reaction, causing degradation of the proton conductor [41]. The content of free hydroxyl groups increased with the increase of THPA content, which reduced the oxidation resistance. The proposed mechanism is shown in Scheme 4.

The hydrolysis resistance of ZrTHPA is shown in Fig. 4(b). After hydrolysis test, the remained weight of ZrTHPA (1:1, 3:4, 2:3, 1:2) was 89%, 92%, 94%, and 97%, respectively. It can be seen from the figure that hydrolysis resistance of the ZrTHPA increased as the THPA content increased. This may be because the ionic bond was formed between Zr and O, and the electron-withdrawing effect reduced the electron cloud density on the phosphorus atom, making it more susceptible to nucleophilic attacked by water molecules, and the Zr ion could catalyze ZrTHPA hydrolysis reaction (of which the content is equivalent rather than catalytic amount). The proposed mechanism is shown in Scheme 5.

Thermogravimetry-differential thermal analysis

The thermogravimetry-differential thermal analysis (TG-DTA) curves of ZrTHPA are shown in Fig. 5(a). According to the TG-DTA spectrum, the weight loss of ZrTHPA (1:2) was 1.05 wt% between room temperature to 200°C . There

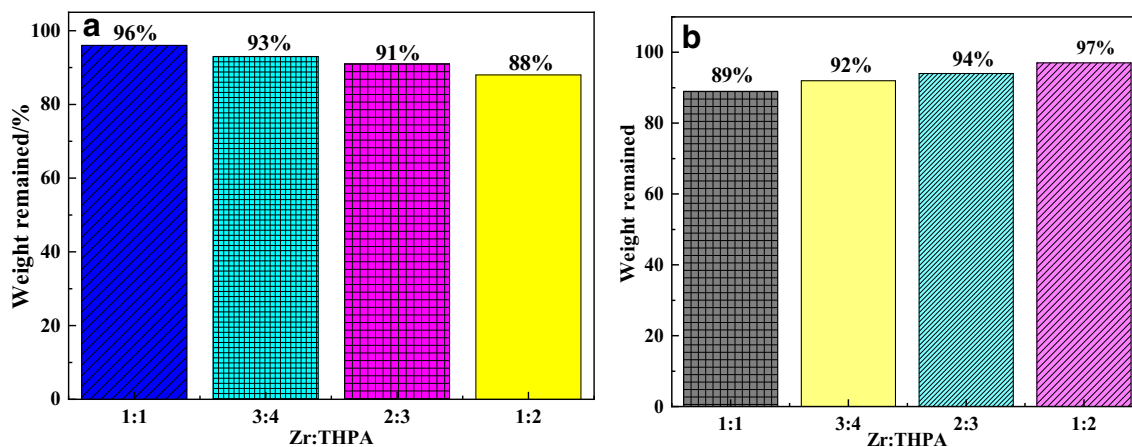
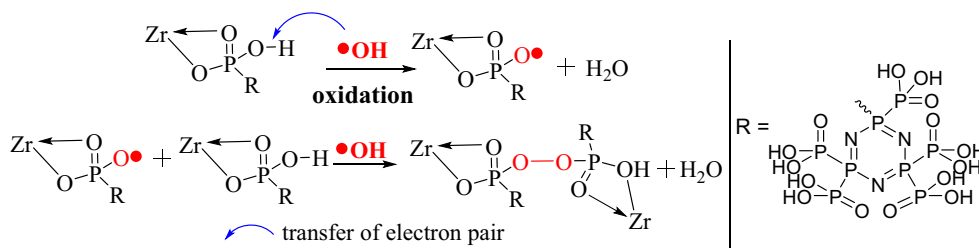


Fig. 4 Fenton test (a) and hydrolysis (b) resistance of ZrTHPA

Scheme 4 The proposed oxidation mechanism of ZrTHPA



was an endothermic peak on the corresponding DTA curve due to the loss of bound water between molecular interlayers. ZrTHPA (1:2) exhibited significant mass loss above 200 °C, which was corresponded to an endothermic peak appeared on the DTA curve caused by the degradation of the organic skeleton. The phosphoric acid groups in ZrTHPA dehydrated to give pyrophosphate. At 798.2 °C, the residual mass of ZrTHPA remained 89.9%, which was significantly better than ZrPA [42] and ZrSPP [38], indicating that ZrTHPA had good thermal stability.

IEC of ZrTHPA

The IEC of ZrTHPA is shown in Table 1. The IEC of ZrTHPA (1:1), ZrTHPA (3:4), ZrTHPA (2:3), and ZrTHPA (1:2) was 1.35, 1.62, 1.86, and 2.21 meq g⁻¹, respectively. The IEC of ZrTHPA increased as the content of THPA increased, because the increase in THPA caused increase in the content of free hydroxyl groups, which increased the IEC. After soaking for 24 h in deionized water at 80 °C of ZrTHPA (1:2), 1.73 g powder was obtained corresponding to the water uptake of 73%.

Proton conductivities of ZrTHPA

The proton conductivity of ZrTHPA was tested at different temperatures and humidity. The results are shown in Fig. 5(b–d). At 100% RH (Fig. 5(b)), the proton conductivity of ZrTHPA (1:2) increased from 0.027 to 0.128 S cm⁻¹ as the temperature increased from 30 to 180 °C, which was higher than that of FeSPP (0.115 S cm⁻¹ at 180 °C) [43]. At 180 °C, the proton conductivity of ZrTHPA (1:1, 3:4, 2:3) was 0.091, 0.104, and 0.115 S cm⁻¹, respectively. At 50% RH (Fig. 5(c)), when the temperature was raised from 100 to 180 °C, the proton conductivity of ZrTHPA (1:2) increased from 0.026

to 0.069 S cm⁻¹, which was higher than that of ZrPA (0.042 S cm⁻¹ at 140 °C) [42]. At 0 RH (Fig. 5(d)), the proton conductivity of ZrTHPA (1:2) raised from 0.0034 to 0.038 S cm⁻¹ from 30 to 180 °C, which was higher than that of LaSPP (1.118 × 10⁻² S cm⁻¹ at 170 °C) [44]. At 180 °C, the proton conductivity of ZrTHPA (1:1, 3:4, 2:3) was 0.028, 0.031, and 0.034 S cm⁻¹, respectively. It can be seen from Fig. 5(b–d) that the proton conductivity of ZrTHPA increased with the increase of temperature, relative humidity (RH), and THPA content. As the temperature increased, the movement of the molecules was accelerated, which facilitated the conduction of protons. Because of the increase of THPA content, ZrTHPA had more phosphonic acid groups bearing hydrogen bond donors and acceptors. Therefore, ZrTHPA can form more intensive hydrogen bond networks, which accelerated proton transport. That explains why ZrTHPA (1:2) had the highest conductivity.

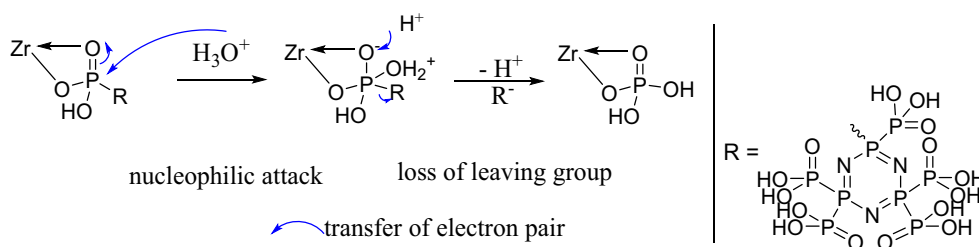
It was found that the logarithm of conductivity was linearly related to temperature. It was known that the kinetics of proton conduction were in good accordance with the Arrhenius equation. The activation energy of proton transfer can be calculated according to the following Arrhenius equation:

$$\sigma = A \exp\left(\frac{E_{act}}{RT}\right)$$

where σ (S cm⁻¹), A , E_{act} (kJ mol⁻¹), R (8.314 J mol⁻¹ K⁻¹), and T (K) are the proton conductivity, pre-exponential factor, activation energy of proton conduction, molar gas constant, and thermodynamic temperature, respectively.

The activation energy for proton conduction was calculated by Arrhenius equation. At 100% RH, the proton conduction activation energy of ZrTHPA (1:1, 3:4, 2:3, 1:2) was 16.88, 14.73, 13.31, and 11.84 kJ mol⁻¹, respectively. With the increase of THPA content, ZrTHPA had more phosphonic acid

Scheme 5 The proposed hydrolysis mechanism of ZrTHPA



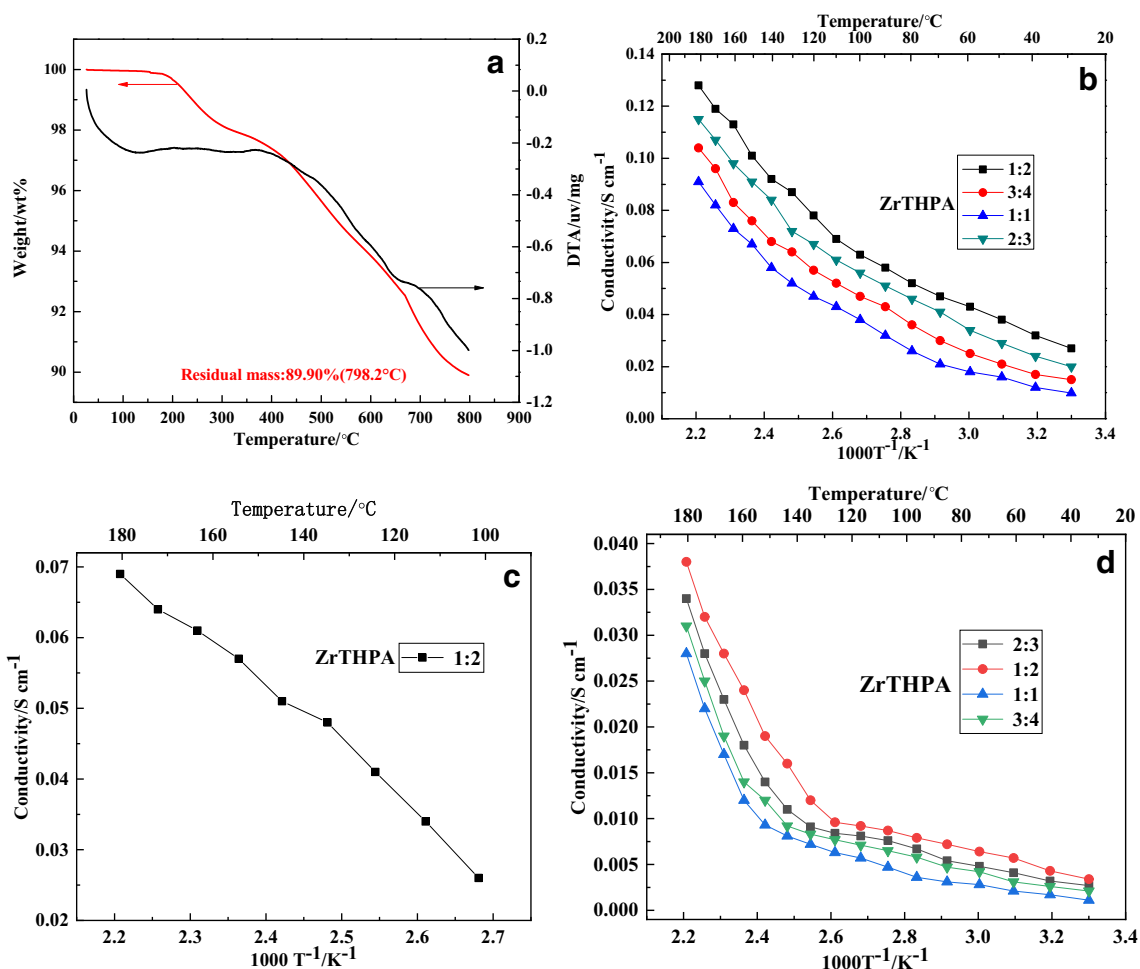


Fig. 5 TG-DTA curves (a) and proton conductivities of ZrTHPA (b: at 100% RH; c: at 50% RH; d: at 0 RH)

groups bearing hydrogen bond donors and acceptors, which accelerated proton transport and reduced activation energy. The proton conduction activation energy of ZrTHPA (1:2) was 17.14 kJ mol^{-1} at 50% RH. At 100% RH, the proton conduction activation energy of ZrTHPA (1:1, 3:4, 2:3, 1:2) was 24.63, 20.48, 19.27, and 18.36 kJ mol^{-1} , respectively.

This was because that proton conduction mainly depended on the vehicle mechanism (in which protons were transferred in the form of hydronium ions) at 100% RH. The sketch of vehicle mechanism of ZrTHPA is shown in Fig. 6(a). When the relative humidity decreased, the activation energy increased. At 50% RH, vehicle mechanism and hopping

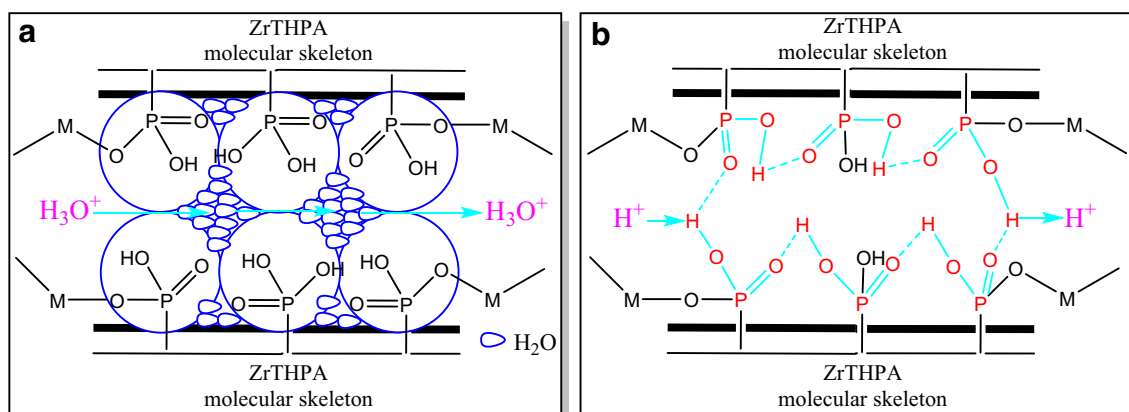


Fig. 6 Vehicle mechanism (a) and hopping mechanism (b) of ZrTHPA

Table 2 Proton conductivity of several proton conductors

Proton conductor	RH	Temperature (°C)	σ (S cm ⁻¹)	Ref.
CeSPP	100%	150	0.13	[45]
FeSPP	0	180	2.15×10^{-3}	[43]
LaSPP	100%	170	0.123	[44]
ZrPA	0	180	0.018	[42]
SPAN	50%	180	0.064	[4]
ionic molecules	0	140	10^{-2}	[46]
(CH ₃ NH ₃) ₂ Ag ₄ Sn ₃ S ₈	99%	70	1.14×10^{-3}	[47]
Im@(NENU-3)	90%	70	1.82×10^{-2}	[48]
ZrTHPA (1:2)	50%	180	0.069	This work
ZrTHPA (1:2)	100%	180	0.128	This work
ZrTHPA (1:2)	0	180	0.028	This work

mechanism coexisted. As the relative humidity decreased, the vehicle mechanism was inhibited due to its water-dependence, and the contribution of the hopping mechanism increased. Under dry conditions, the proton conduction activation energy became larger, and proton conduction relied on the hopping mechanism. The sketch of hopping mechanism of ZrTHPA is shown in Fig. 6(b). From the point of view of the hopping mechanism, proton conduction took place through consecutive breaking and formation of hydrogen bonds. Because proton conduction needs to overcome higher energy barriers under the hopping mechanism, the activation energy under dry conditions was the highest. In summary, the activation energy of proton conduction increased with decreased relative humidity.

The proton conductivity of the proton conductors is shown in Table 2. By comparison, ZrTHPA had better proton conductivity and could be used as a proton conductor.

Conclusions

ZrTHPA was synthesized as a novel high-temperature proton conductor. It had a layered structure from SEM and XRD. It exhibited good thermal stability up to 200 °C and the remaining weight percentage was 89% at 800 °C from TG. ZrTHPA (1:2) presented the weight loss of 12% after Fenton test for 24 h at 68 °C and the weight loss of 3% after hydrolysis test for 24 h at 80 °C. ZrTHPA demonstrated good oxidative stability and hydrolysis resistance. This proton conductor had intensive hydrogen bonds. The ion exchange capacity of ZrTHPA (1:2) was 2.21 meq g⁻¹ and the conductivity of ZrTHPA (1:2) at 100% RH, 50% RH and 0 RH was 0.128 S cm⁻¹, 0.069 S cm⁻¹, and 0.038 S cm⁻¹ at 180 °C, respectively.

Funding This work was financially supported by the National Natural Science Foundation of China (Grant Nos. 21776167 and 21276148),

Natural Science Foundation of Shandong Province, China (Grant No. ZR2019QB012), Zibo City School-City Integration Development Project (Grant No. 2019ZBXC411), and the State Key Laboratory of Chemical Engineering (Tianjin University) (Grant No. SKL-ChE-14B01).

References

- Ossiander T, Perchthaler M, Heinzl C, Schönberger F, Völk P, Welsch M, Chromik A, Hacker V, Scheu C (2016) Influence of membrane type and molecular weight distribution on the degradation of PBI-based HTPeM fuel cells. *J Membr Sci* 509:27–35
- Wang C, Li Z, Wang L, Niu X, Wang S (2019) Facile synthesis of 3D Fe/N codoped mesoporous graphene as efficient bifunctional oxygen electrocatalysts for rechargeable Zn–air batteries. *ACS Sustain Chem Eng* 7:13873–13885
- Wei Y, Qian T, Liu J, Guo X, Gong Q, Liu Z, Tian B, Qiao J (2019) *J Mater* 5:252
- Sun P, Li Z, Wang S, Yin X (2018) Performance enhancement of polybenzimidazole based high temperature proton exchange membranes with multifunctional crosslinker and highly sulfonated polyaniline. *J Membr Sci* 549:660–669
- Ranjani M, Yoo DJ, Kumar GG (2018) Sulfonated Fe₃O₄@SiO₂ nanorods incorporated sPVdF nanocomposite membranes for DMFC applications. *J Membr Sci* 555:497–506
- Lv YA, Li ZF, Song MF, Sun P, Yin XY, Wang SW (2019) Preparation and properties of ZrPA doped CMPSU cross-linked PBI based high temperature and low humidity proton exchange membranes. *React Funct Polym* 137:57–70
- Yang J, Wang Y, Yang G, Zhan S (2018) New anhydrous proton exchange membranes based on fluoropolymers blend imidazolium poly (aromatic ether ketone)s for high temperature polymer electrolyte fuel cells. *Int J Hydrog Energy* 43:8464–8473
- Wang S, Sun P, Hao X, Li Z, Liu G, Jin L, Yin X (2018) Ferric sulfophenyl phosphate bonded with phosphotungstic acid as a novel intercalated high-temperature inorganic-organic proton conductor. *Mater Chem Phys* 213:35–43
- Trigg EB, Gaines TW, Maréchal M, Moed DE, Rannou P, Wagener KB, Stevens MJ, Winey KI (2018) Self-assembled highly ordered acid layers in precisely sulfonated polyethylene produce efficient proton transport. *Nat Mater* 17:725–731
- Won S, Oh K, Ju H (2016) Numerical degradation studies of high-temperature proton exchange membrane fuel cells with phosphoric acid-doped PBI membranes. *Int J Hydrog Energy* 41:8296–8306

11. Sun H, Yu M, Zhao X, Almheiri S (2016) Molecular simulation of mass transport in phosphoric acid doped poly(2,5-benzimidazole) polymer electrolyte membranes. *Int J Hydrog Energy* 41:7614–7621
12. Han S, Jeong YH, Jung JH, Begley A, Choi E, Yoo SJ, Jang JH, Kim H-J, Nam SW, Kim JY (2016) *J Sensors* 2016:8
13. Subianto S (2014) Recent advances in polybenzimidazole/phosphoric acid membranes for high-temperature fuel cells. *Polym Int* 63:1134–1144
14. Kumar AG, Singh A, Komber H, Voit B, Tiwari BR, Noori MT, Ghangrekar MM, Banerjee S (2018) Novel sulfonated copoly(ether imide)s containing trifluoromethyl, fluorenyl and hydroxyl groups for enhanced proton exchange membrane properties: application in microbial fuel cell. *ACS Appl Mater Interfaces* 10:14803–14817
15. Kim K, Jung B-K, Ko T, Kim T-H, Lee J-C (2018) Comb-shaped polysulfones containing sulfonated polytriazole side chains for proton exchange membranes. *J Membr Sci* 554:232–243
16. Hu H, Dong T, Sui Y, Li N, Ueda M, Wang L, Zhang X (2018) A thermally crosslinked multiblock sulfonated poly(arylene ether ketone nitrile) copolymer with a 1,2,3-triazole pendant for proton conducting membranes. *J Mater Chem A* 6:3560–3570
17. Sondergaard T, Cleemann LN, Becker H, Aili D, Steenberg T, Hjuler HA, Seerup L, Li Q, Jensen JO (2017) Long-term durability of HT-PEM fuel cells based on thermally cross-linked polybenzimidazole. *J Power Sources* 342:570–578
18. Chen X, Xu H, Liu D, Yan C, Zhu Y (2019) A novel and facile fabrication of polyphosphazene nanotube/carbon fiber multi-scale hybrid reinforcement and its enhancing effect on the interfacial properties of epoxy composites. *Compos Sci Technol* 169:34–44
19. Saithong N, Authayanun S, Patcharavorachot Y, Arpornwichanop A (2019) Thermodynamic analysis of the novel chemical looping process for two-grade hydrogen production with CO₂ capture. *Energy Convers Manag* 180:325–337
20. Zhang X, Liu Q, Xia L, Huang D, Fu X, Zhang R, Hu S, Zhao F, Li X, Bao X (2019) Poly(2,5-benzimidazole)/sulfonated sepiolite composite membranes with low phosphoric acid doping levels for PEMFC applications in a wide temperature range. *J Membr Sci* 574:282–298
21. Zeng J, He B, Lamb K, De Marco R, Shen PK, Jiang SP (2013) Anhydrous phosphoric acid functionalized sintered mesoporous silica nanocomposite proton exchange membranes for fuel cells. *ACS Appl Mater Interfaces* 5:11240–11248
22. Zhao Y, Li X, Wang S, Li W, Wang X, Chen S, Chen J, Xie X (2017) Proton exchange membranes prepared via atom transfer radical polymerization for proton exchange membrane fuel cell: recent advances and perspectives. *Int J Hydrog Energy* 42:30013–30028
23. Weikel AL, Cho SY, Morozowich NL, Nair LS, Laurencin CT, Allcock HR (2010) Hydrolysable polylactide–polyphosphazene block copolymers for biomedical applications: synthesis, characterization, and composites with poly(lactic-co-glycolic acid). *Polym Chem* 1:1459
24. Yang J, Liu C, Gao L, Wang J, Xu Y, Wang T, He R (2016) Phosphoric acid doped imidazolium silane crosslinked poly(epichlorohydrin)/PTFE as high temperature proton exchange membranes. *RSC Adv* 6:61029–61036
25. Wycisk R, Pintauro PN (2008) in *Fuel Cells II*, p. 157
26. Xu X, Wang H, Lu S, Guo Z, Rao S, Xiu R, Xiang Y (2015) A novel phosphoric acid doped poly(ethersulphone)-poly(vinyl pyrrolidone) blend membrane for high-temperature proton exchange membrane fuel cells. *J Power Sources* 286:458–463
27. Cao L, Wu H, Mu Z, He X, Wang C, Li J, Li Y, Xu M, Jiang Z (2018) Phosphorylated graphene monoliths with high mixed proton/electron conductivity. *J Mater Chem A* 6:8499–8506
28. Yamaguchi T, Kataoka T, Tsukuda S, Ishiyama T, Nishii J, Yamashita T, Kawazoe H, Omata T (2017) The mobility of proton carriers in phosphate glasses depends on polymerization of the phosphate framework. *PCCP* 19:29669–29675
29. Ozden A, Ercelik M, Devrim Y, Colpan CO, Hamdullahpur F (2017) Evaluation of sulfonated polysulfone/zirconium hydrogen phosphate composite membranes for direct methanol fuel cells. *Electrochim Acta* 256:196–210
30. Rezakazemi M, Sadrzadeh M, Matsuura T (2018) Thermally stable polymers for advanced high-performance gas separation membranes. *Prog Energy Combust Sci* 66:1–41
31. Qiu S, Ma C, Wang X, Zhou X, Feng X, Yuen RKK, Hu Y (2018) Melamine-containing polyphosphazene wrapped ammonium polyphosphate: a novel multifunctional organic-inorganic hybrid flame retardant. *J Hazard Mater* 344:839–848
32. Ouadah A, Luo T, Gao S, Zhu C (2018) Controlling the degree of sulfonation and its impact on hybrid cross-linked network based polyphosphazene grafted butylphenoxy as proton exchange membrane. *Int J Hydrog Energy* 43:15466–15480
33. Fiedler C, Luerssen B, Lucht B, Janek J (2018) Synthesis and characterization of polyphosphazene electrolytes including cyclic ether side groups. *J Power Sources* 384:165–171
34. Dar SU, Ud Din MA, Hameed MU, Ali S, Akram R, Wu Z, Wu D (2018) Oxygen reduction reaction of (C-PCTNB@CNTs): a nitrogen and phosphorus dual-doped carbon electro-catalyst derived from polyphosphazenes. *J Power Sources* 373:61–69
35. Chen X, Xu H, Liu D, Yan C, Zhu Y (2017) A facile one-pot fabrication of polyphosphazene microsphere/carbon fiber hybrid reinforcement and its effect on the interfacial adhesion of epoxy composites. *Appl Surf Sci* 410:530–539
36. Song M, Lu X, Li Z, Liu G, Yin X, Wang Y (2016) Compatible ionic crosslinking composite membranes based on SPEEK and PBI for high temperature proton exchange membranes. *Int J Hydrog Energy* 41:12069–12081
37. Byczyński Ł, Dutkiewicz M, Januszewski R (2017) Thermal behaviour and flame retardancy of polyurethane high-solid coatings modified with hexakis(2,3-epoxypropyl)cyclotriphosphazene. *Prog Org Coat* 108:51–58
38. Wang S, Jin L, Li Z (2012) *Ionics* 19:1027
39. Alidağ HA, Gırgıç ÖM, Zorlu Y, Hacivelioglu F, Çelik SÜ, Bozkurt A, Kılıç A, Yeşilot S (2013) Synthesis and proton conductivity of azole-substituted cyclic and polymeric phosphazenes. *Polymer* 54:2250–2256
40. Liu P, Li C, Liang X, Xu J, Lu G, Ji F (2013) Advanced oxidation of hypophosphite and phosphite using a UV/H₂O₂ process. *Environ Technol* 34:2231–2239
41. Huang Y-H, Su H-T, Lin L-W (2009) Removal of citrate and hypophosphite binary components using Fenton, photo-Fenton and electro-Fenton processes. *J Environ Sci* 21:35–40
42. Sun P, Li Z, Song M, Wang S, Yin X, Wang Y (2017) Preparation and characterization of zirconium phytate as a novel solid intermediate temperature proton conductor. *Mater Lett* 191:161–164
43. Liu G, Li Z, Jin L, Wang S (2014) Simple synthesis of ironIII sulfophenyl phosphate nanosheets as a high temperature inorganic–organic proton conductor. *Ionics* 20:1399–1406
44. Liu C, Yan H, Lv Q, Li S, Niu S (2016) Enhanced tribological properties of aligned reduced graphene oxide-Fe₃O₄@polyphosphazene/bismaleimides composites. *Carbon* 102:145–153
45. Dong F, Li Z, Wang S, Wang Z (2011) Cerium sulfophenyl phosphate, a novel inorgano–organic solid proton-conducting material. *Mater Lett* 65:1431–1433

46. Kumar A, Pisula W, Sieber C, Klapper M, Mullen K (2018) Anhydrous proton conduction in self-assembled and disassembled ionic molecules. *J Mater Chem A* 6:6074–6084
47. Luo H-B, Wang M, Zhang J, Tian Z-F, Zou Y, Ren X-M (2018) Open-framework chalcogenide showing both intrinsic anhydrous and water-assisted high proton conductivity. *ACS Appl Mater Interfaces* 10:2619–2627
48. Ye Y, Guo W, Wang L, Li Z, Song Z, Chen J, Zhang Z, Xiang S, Chen B (2017) Straightforward loading of imidazole molecules into metal–organic framework for high proton conduction. *J Am Chem Soc* 139:15604–15607

Publisher's note Springer Nature remains neutral with regard to jurisdictional claims in published maps and institutional affiliations.